$CeRu_2Al_2B$: A local-moment $4f$ magnet with a complex T-H phase diagram

R. E. Baumbach,[1] H. Chudo,[1,2] H. Yasuoka,[1,2] F. Ronning,[1] E. D. Bauer,[1] and J. D. Thompson[1]
[1]*MPA-CMMS Los Alamos National Laboratory, Los Alamos, New Mexico 87545, USA*
[2]*Advanced Science Research Center, Japan Atomic Energy Agency, Tokai, Ibaraki, Japan*
(Received 24 January 2012; revised manuscript received 5 March 2012; published 22 March 2012)

The temperature-magnetic field (T-H) phase diagram for the tetragonal compound $CeRu_2Al_2B$, determined from magnetization, specific heat, nuclear magnetic resonance (NMR), and electrical resistivity is reported. This system exhibits localized $4f$ magnetic ordering at high temperatures where antiferromagnetism is observed at a Néel temperature $T_N = 14.2$ K and a first-order ferromagnetic transition is observed at a Curie temperature $T_C = 12.8$ K. The application of a magnetic field H results in a rich phase diagram that includes three magnetically ordered phases: (1) antiferromagnetic, (2) canted antiferromagnetic, and (3) ferromagnetic, indicating that there are several finely tuned exchange interactions.

DOI: 10.1103/PhysRevB.85.094422 PACS number(s): 75.50.Cc, 75.50.Ee, 71.27.+a

I. INTRODUCTION

A variety of emergent phenomena are observed in compounds that include transition metal, lanthanide, and actinide elements, due to the presence of d- or f-electron states, which are remarkably tunable in their capacity to hybridize with conduction electron states.[1–4] Research on such systems has led to a point of view that is summarized by the Doniach phase diagram, where the tendency of the d or f electrons to localize or delocalize is driven by a competition between the RKKY and Kondo interactions.[5,6] In this framework, an interesting situation arises at the point where a continuous magnetic phase transition is suppressed to zero temperature as a result of hybridization, i.e., at a quantum critical point (QCP).[7–10] Here, a variety of phenomena are often seen including unconventional superconductivity (SC)[3] and non-Fermi liquid (NFL) behavior.[1,2]

In conjunction with the development of the Doniach picture and studies of quantum criticality, certain types of crystal structures have proven to be a common theme (e.g., $ThCr_2Si_2$ and $HoCoGa_5$ type), suggesting that the details of the d- or f-electron element environment play a significant role in how the physical state emerges. For this reason, we were motivated to explore the possible existence of $4f$-electron versions of $LaRu_2Al_2B$. This compound forms in a chemical variant of the tetragonal $CeCr_2Si_2C$ prototype (a stuffed version of the $CeMg_2Si_2$ structure type) and can be viewed as an alternative stacking arrangement of the $ThCr_2Si_2$ structure.[11] We subsequently synthesized $CeRu_2Al_2B$, which exhibits localized $4f$ magnetic ordering at high temperatures; antiferromagnetism (AFM) develops below a Néel temperature $T_N = 14.2$ K and a first-order ferromagnetic (FM) transition is observed at a Curie temperature $T_C = 12.8$ K. The application of a magnetic field H results in a phase diagram that includes three magnetically ordered phases: (1) AFM, (2) canted AFM, and (3) FM where the transition for low H is first order and becomes weakly first order with increasing H.

This type of magnetism is unusual for compounds that include Ce, although similar behavior is often observed for heavy rare-earth elements.[12] Some well-known exceptions are CeSb,[13] $CeIn_2$,[14,15] $CeRu_2Ge_2$, and $CeRu_2Ge_{2-x}Si_x$,[16–18] each of which exhibits complicated magnetic phase diagrams as a function of various tuning parameters. As such, $CeRu_2Al_2B$ belongs to a small group of Ce-based compounds where finely tuned exchange interactions drive the emergence of varied magnetic configurations as a function of a tuning parameter (e.g., T, H, and pressure P). This situation raises the interesting possibility that quantum frustration (QF) may occur in $CeRu_2Al_2B$, which would be noteworthy since a tetragonal lattice does not promote QF from a geometrical point of view. Moreover, the importance of QF in correlated electron systems recently was emphasized by the theoretical work of Si and Coleman.[19,20]

It is additionally significant that while AFM-QC has received a great deal of attention, the possible existence of FM-QC is also of interest. However, materials that are suitable for studying FM-QC are uncommon. In addition to those listed above, CePt,[21] $CeSi_x$,[22] $CeAgSb_2$,[23] and CeRuPO[24] have attracted interest in this context. Some U-based ferromagnets, including UGe_2,[25] URhGe,[26] and UIr,[27] have also been intensely studied because they exhibit a dome of SC in the vicinity of the region where FM is suppressed. We note that some systems that show "prototypical" AFM-QC (e.g., $YbRh_2Si_2$[28,29]) may exhibit FM fluctuations near their QCP. For these reasons, further study of FM compounds like $CeRu_2Al_2B$ in the context of QC is highly desirable, as pointed out by the recent theoretical work of Yamamoto and Si.[30]

II. EXPERIMENTAL DETAILS

Polycrystalline specimens of $LnRu_2Al_2B$ (Ln = La–Sm) were synthesized by arc melting stoichiometric quantities of Ln (99.99%), Ru (99.99%), Al(99.999%), and B (99.5%) under an Ar atmosphere. The resulting boules were flipped and remelted several times in order to encourage homogeneity and, subsequently, annealed in evacuated quartz tubes at 900 °C for two weeks. X-ray diffraction (XRD) measurements were performed on powdered specimens. The resulting patterns were fitted by means of Rietveld analysis[31] implemented in the program suite GSAS[32] and shown to agree with the $LaRu_2Al_2B$ structure. For Ln = Ce, the lattice constants are $a = b = 4.198$ Å and $c = 5.607$ Å. As shown in Fig. 1, the unit cell volume for $CeRu_2Al_2B$ coincides with the observed lanthanide contraction for $LnRu_2Al_2B$ (Ln = La–Sm), suggesting that the Ce ions are in the 3+ valence state.

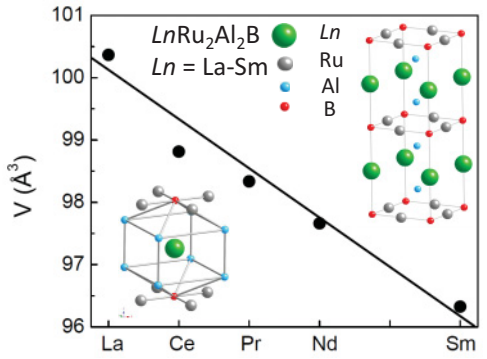

FIG. 1. (Color online) Unit cell volumes for the compounds $Ln\mathrm{Ru_2Al_2B}$ (Ln = La–Sm). Also shown are two unit cells of the $Ln\mathrm{Ru_2Al_2B}$ structure (top right inset) and the nearest-neighbor environment for the Ln ions (bottom left inset).

Magnetization $M(T,H)$ measurements were carried out for temperatures T = 2–300 K under applied magnetic fields H = 0.01–10 kOe and T = 2–14 K up to H = 50 kOe, respectively, using a quantum design magnetic property measurement system. The specific heat $C(T,H)$ was measured for T = 2–300 K up to H = 30 kOe and the electrical resistivity $\rho(T,H)$ was measured for T = 0.4–300 K up to H = 90 kOe using a quantum design physical property measurement system. Frequency swept nuclear magnetic resonance (NMR) spectra were taken at several temperatures by enveloping the fast Fourier transformation of spin-echo profiles obtained at each frequency.

III. RESULTS

Shown in Fig. 2 is the T-H phase diagram for $\mathrm{CeRu_2Al_2B}$, which we have constructed based on the measurements discussed below. We find that for small magnetic fields there are two well defined magnetic phase transitions that emerge from the paramagnetic high-T state; a second-order AFM phase transition occurs near T_N = 14.2 K and is rapidly followed by a first-order FM transition near T_C = 12.8 K. Measurements of $M(H)$ and $C(T)/T$ show that these transitions are associated with localized Ce ions for which the Hund's rule multiplet is split by the crystalline electric field, resulting in a doublet ground state. An applied magnetic field separates the ordered phase space into three distinct regions. With increasing H, T_N remains roughly constant up to H = 0.4 kOe and appears to slowly decrease for larger H, although it becomes difficult to track. We also find that up to H = 30 kOe, the FM ordering temperature decreases slowly, after which it is also difficult to define due to the broadness of the transition, although a FM ground state clearly persists. Finally, measurements of $M(H)$, $\rho(H)$, and $\rho(T)$ reveal a line that connects the zero-field FM state to the applied field AFM state. This line represents an abrupt transformation from the low-H AFM to a spin reoriented state, which is FM in nature, but distinct from the low-T FM. For this reason, we suggest that it is a canted AFM.

The $M(T)/H$ and $M(H)$ data are summarized in Figs. 3 and 4, where complicated magnetic ordering is evident. As shown in Fig. 3(b), modified Curie-Weiss (CW) behavior given

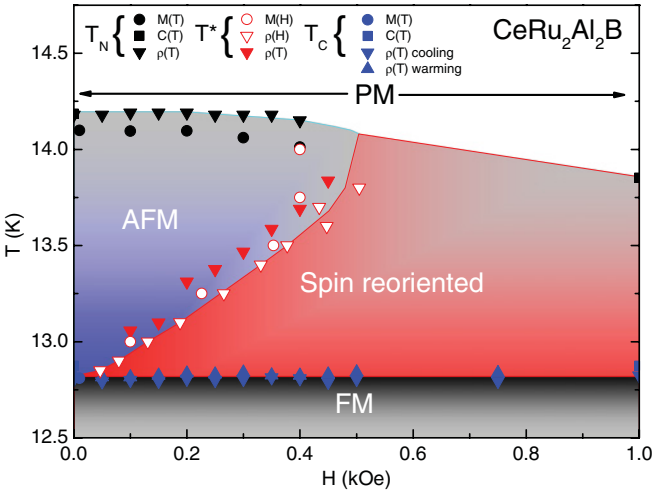

FIG. 2. (Color online) Temperature T vs magnetic field H phase diagram for $\mathrm{CeRu_2Al_2B}$ constructed from the magnetization M, specific heat C, and electrical resistivity ρ data. The upper phase boundary $T_N(H)$ separates the paramagnetic state from the antiferromagnetic (AFM) and canted AFM (see text) states. The diagonal boundary that connects the zero H ferromagnetic (FM) state and the AFM state shows the values of H where a transformation from AFM to canted AFM occurs. The lower boundary represents the FM ordering Ts.

by the expression,

$$\chi(T) = \chi_0 + C/(T - \Theta) \qquad (1)$$

is observed in the high-T region, where $\chi_0 = 0.0015\,\mathrm{cm^3/mol}$, Θ = 14.5 K, and the Curie constant C yields an effective magnetic moment $\mu_{\mathrm{eff}} \approx 2.45\ \mu_B$, which is close to what is expected for Ce^{3+} ions. Although χ_0 is unusually large, we point out that the homologous compound without $4f$

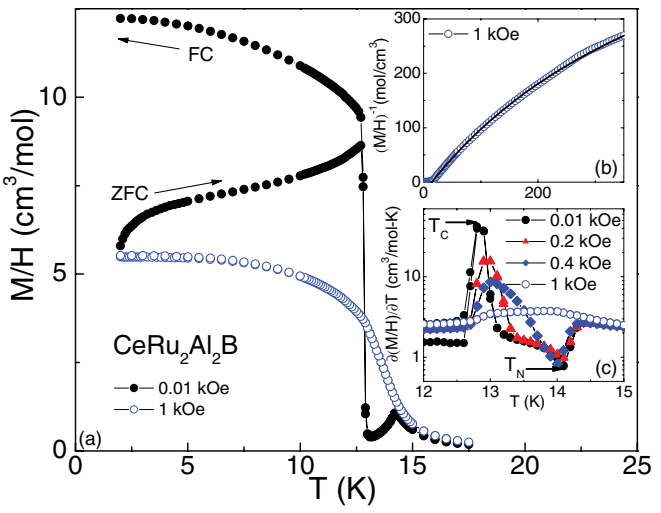

FIG. 3. (Color online) (a) Magnetization divided by magnetic field M/H vs temperature T in several H. Zero field cooled (ZFC) and field cooled (FC) curves are shown. (b) M/H^{-1} vs T. The solid line is a modified Curie-Weiss fit to the data [see Eq. (1)]. (c) Derivative of the M/H with respect to T $\partial(\mathrm{M/H})/\partial T$ vs T (offset along the y axis for clarity). Antiferromagnetic and ferromagnetic ordering are observed at T_N and T_C, respectively.

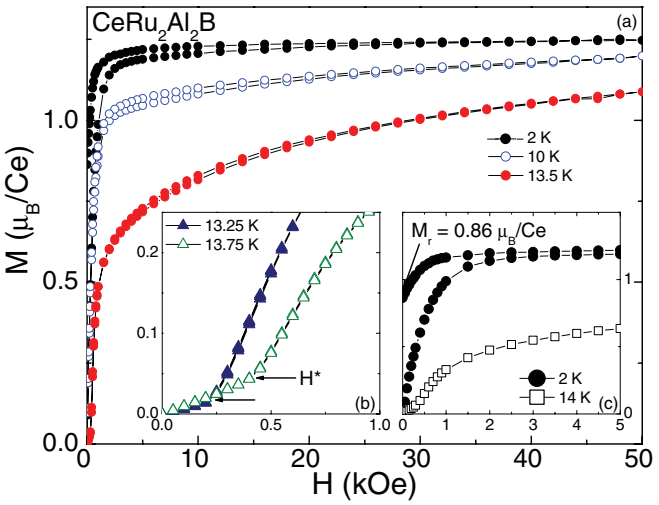

FIG. 4. (Color online) (a) Magnetization M vs magnetic field H at several temperatures T. (b) M vs H at low fields for representative curves where $T_C \leqslant T \leqslant T_N$. The kink denoted as H^* represents a crossover from the low-H AFM state to the canted AFM state, as discussed in the text. (c) M vs H for representative curves where $T \leqslant T_C$ and $T \approx T_N$. For $T \leqslant T_C$, hysteresis is observed in $M(H)$.

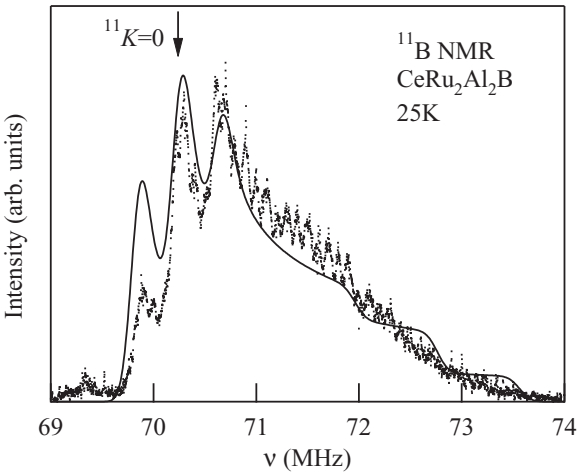

FIG. 5. ^{11}B NMR spectrum in CeRu$_2$Al$_2$B at 25K under an external magnetic field of $H_0 = 5.1419$ T. The solid curve is the best simulated powder pattern in Eq. (2) where ν_Q, $K_\parallel$, and $K_\perp$ are 0.8 MHz, 3.6% and 0%, respectively, and a Gaussian distribution with full width at half maximum of 0.2 MHz was convoluted.

electrons, LaRu$_2$Al$_2$B, also exhibits a large value of χ_0 (see Ref. 11). Such behavior may reflect a large density of states near the Fermi energy arising from the Ru ions. Two features subsequently emerge at low T [see Fig. 2(a)]; (1) an AFM transition near $T_N = 14.2$ K and (2) a hysteretic FM transition near $T_C = 12.8$ K. The application of a small magnetic field immediately reduces the hysteresis and causes the two transitions to begin to overlap, as emphasized by $\partial(M/H)/\partial T$ [see Fig. 3(c)]. For fields above 1 kOe, two distinct transitions are no longer observable in $M(T)/H$ and the magnetic state is predominantly FM in character, although close inspection of $\partial(M/H)/\partial T$ reveals additional features that may be related to the spin reconfiguration.

Measurements of the isothermal magnetization $M(H)$ provide further insight into the magnetic behavior. For $T \leqslant T_C$ [see Figs. 4(a) and 4(c)], $M(H)$ is hysteretic and saturates rapidly with increasing H, e.g, $M_s(2\text{ K}) = 1.24\mu_B$/Ce. Taken together, these data show that at low T, the Ce ion spins are well localized and arranged ferromagnetically. Additionally, the value of M_s suggests that the Hund's rule multiplet for the Ce ions is split by the crystal electric field, resulting in a doublet ground state. For $T_C \leqslant T \leqslant T_N$, $M(H)$ initially increases linearly at low fields, consistent with an AFM configuration [see Fig. 4(b)]. The magnetization then evolves through a kink, denoted as H^*, after which $M(H)$ increases dramatically. This behavior indicates that along the phase line defined by H^*, the Ce ion spins undergo a reconfiguration from AFM to an arrangement that more closely resembles FM.

In order to investigate the microscopic magnetic properties of CeRu$_2$Al$_2$B, the ^{11}B NMR was measured in both the paramagnetic and FM states using a powdered sample. Here, we confine ourselves to a discussion of results for the paramagnetic state. As a typical example, the frequency swept ^{11}B NMR in an external magnetic field of 5.1419 T and at 25 K is shown in Fig 5. Since the B atoms in CeRu$_2$Al$_2$B occupy crystallographically equivalent sites with tetragonal symmetry, the NMR spectrum is expected to be composed of a combined effect of the anisotropic magnetic shift and the nuclear quadrupole interaction for ^{11}B ($I = 3/2$). In order to analyze the observed powder spectrum, we adopted the first-order perturbation formula for the quadrupole splitting with axial symmetry. The angular dependence of the resonance frequency for the mth quadrupole transition may be written as

$$\nu_m(\theta) = \nu_0(1 + K_\parallel \cos^2\theta + K_\perp \sin^2\theta) + \tfrac{1}{2}\nu_Q\left(m + \tfrac{1}{2}\right)(3\cos^2\theta - 1), \quad (2)$$

where ν_0 and ν_Q are the Zeeman and the nuclear quadrupolar frequencies, respectively, θ is the angle between the external field and the crystalline c axis, and $K_\parallel$ and $K_\perp$ are the Knight shifts parallel and perpendicular to the c axis, respectively.[33] The subscript m in Eq. (2) represents the transition between $(m + 1)$th and mth levels: $m = 1/2$, $-1/2$, and $-3/2$ for ^{11}B. According to the standard procedure for calculating a powder pattern, we found the best simulation to the data as shown by the solid curve in Fig. 5. The obtained values of ν_Q, $K_\parallel$, and $K_\perp$ are 0.8 MHz, 3.6% and 0%, respectively. It should be noted that the anisotropy in the Knight shift is quite large with $K_\perp$ being almost zero. We also found the temperature dependence of $K_\parallel$ has a Curie-Weiss-like increase with decreasing temperature, but $K_\perp$ remains constant with temperature. This means that the magnetism of CeRu$_2$Al$_2$B is strongly anisotropic, having an Ising-like nature with the c axis being the easy axis. Further experiments using a single crystal are necessary to make additional quantitative statements.

The specific heat divided by temperature C/T data is shown in Fig. 6. The evolution of C/T for $T \geqslant T_N$ is in close agreement with that of the nonmagnetic analog LaRu$_2$Al$_2$B, showing that in this T region the phonon contribution to C/T is the dominant term [see Fig. 6(a)]. At $T_N = 14.2$ K, a second-order transition that coincides with results from $\chi(T)$ is observed. This feature is followed at $T_C = 12.8$ K by a sharp peak in C/T ($\Delta C/T = 3.35$ J/mol K^2) revealing that this transition is first order in nature. The data at low T are

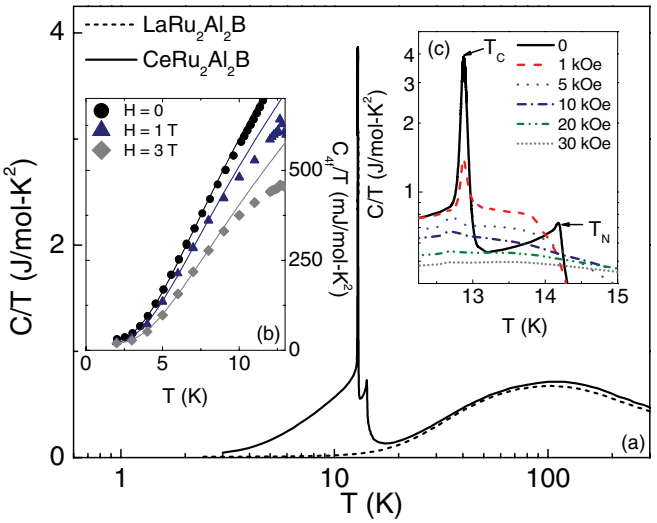

FIG. 6. (Color online) (a) Specific heat divided by temperature C/T vs T for $CeRu_2Al_2B$ and its nonmagnetic analog $LaRu_2Al_2B$. (b) $4f$ contribution to the specific heat C_{4f}/T at low temperatures. The solid lines are fits to the data, as described in the text. (c) C/T vs T in several applied fields H. The antiferromagnetic and ferromagnetic ordering temperatures (T_N and T_C) are evident as a shoulder and a large peak, respectively.

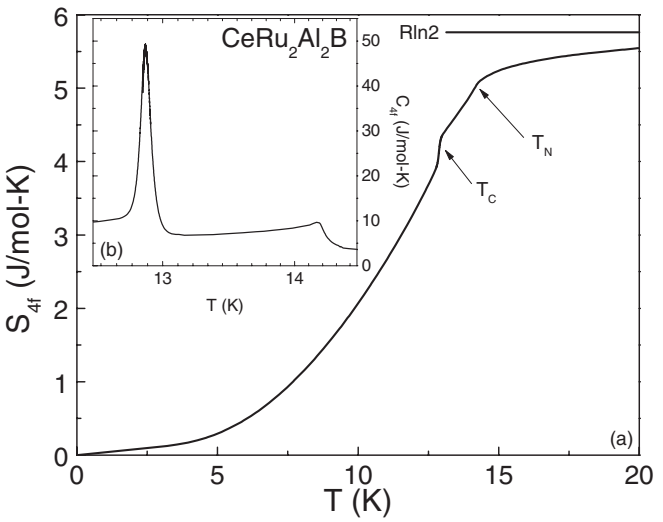

FIG. 7. (a) The $4f$ electron entropy S_{4f} vs temperature T for magnetic field $H = 0$. The antiferromagnetic transition temperature T_N is evident as a broad shoulder, while the ferromagnetic transition temperature T_C appears as a steep increase. (b) The $4f$ electron portion of the specific heat C_{4f} vs T. S_{4f} and C_{4f} were obtained as described in the text.

described by the expression

$$C_{\rm tot}/T = (C_{\rm el} + C_{\rm ph} + C_m)/T, \qquad (3)$$

where $C_{\rm el} = \gamma T$, $C_{\rm ph}$, and C_m are the electronic, lattice, and magnetic contributions, respectively. The magnetic contribution is given by

$$C_m = \beta(\Delta^2/\sqrt{T} + 3\Delta\sqrt{T} + 5\sqrt{T^3})\exp(-\Delta/T), \qquad (4)$$

where β is a fitting constant and Δ is the ferromagnetic magnon gap.[34] In order to fit the data, the phonon contribution was removed by subtracting $C_{\rm La}(T)/T$ for the nonmagnetic analog $LaRu_2Al_2B$, yielding the $4f$ contribution to the specific heat C_{4f}/T. Below $T = 7$ K, the data are well described by Eq. (3) [see Fig. 6(b)]. The resulting fit parameters are summarized in Table I where, for zero field, $\beta = 74.8$ mJ/mol K, $\Delta = 17.6$ K, and $\gamma = 25.6$ mJ/mol K^2. This value for γ indicates that there is little hybridization between the Ce f-electron states and the conduction electron states, which would result in an enhancement of the quasiparticle effective mass.

As shown in Fig. 6(c), T_N rapidly broadens under an applied magnetic field but is still observable up to at least 5 kOe. We also find that increasing H strongly suppresses the magnitude of the feature at T_C, but only weakly suppresses the value of T_C. In fact, the anomaly at T_C persists as high as $H = 30$ kOe.

In order to determine the $4f$ electron contribution to the entropy $S_{4f}(T)$ [see Fig. 7(a)], we subtracted C/T for $LaRu_2Al_2B$ from that of $CeRu_2Al_2B$. We find that $S_{4f}(T)$ increases abruptly at T_C, as expected for a first-order transition, and subsequently, reaches $0.88R \ln 2$ at T_N, further supporting the point of view that the Ce ions are localized and that the crystalline electric field splits the Hund's rule multiplet, resulting in a doublet ground state. $S_{4f}(T)$ reaches approximately $R \ln 6$ near room temperature, as is expected if the entire Hund's rule multiplet becomes populated.

Finally, we investigated the T and H dependence of the electrical resistivity (see Figs. 8 and 9). At $T = 300$ K and $H = 0$, $\rho(T)$ is enhanced by comparison to $LaRu_2Al_2B$, most likely as a result of magnetic scattering from the Ce ions [see Fig. 8(b)]. With decreasing T, $\rho(T)$ initially exhibits negative curvature, which may be ascribed to crystal electric field effects. The electrical resistivity then becomes roughly constant, goes through a weak peak above T_N, exhibits a smooth decrease at T_N, and then decreases abruptly near T_C.

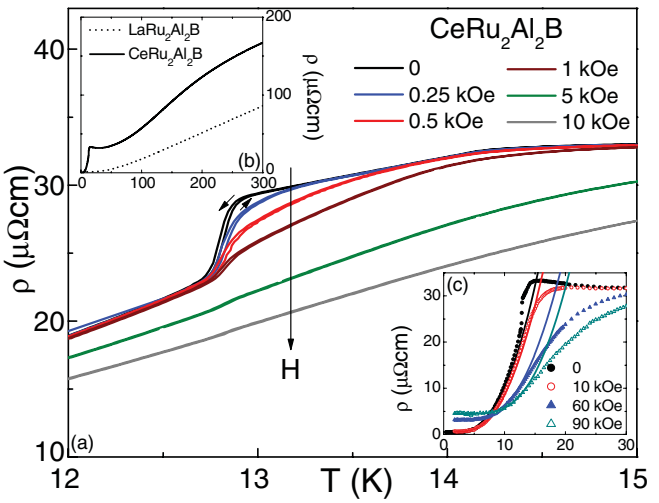

FIG. 8. (Color online) (a) Electrical resistivity ρ vs temperature T in selected magnetic fields H. The arrows denote the field cooling and field warming curves. (b) Comparison between $\rho(T)$ for $CeRu_2Al_2B$ and its nonmagnetic analog $LaRu_2Al_2B$. (c) $\rho(T)$ in constant H. The solid lines are fits to the data using Eq. (5).

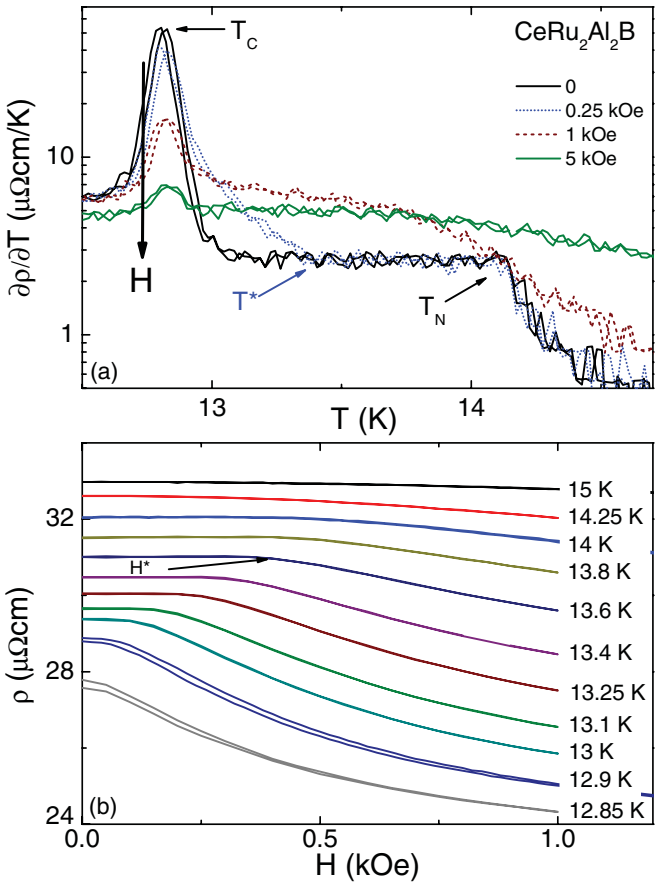

FIG. 9. (Color online) (a) Derivative of the electrical resistivity with respect to temperature $\partial\rho/\partial T$ vs T for selected H. The antiferromagnetic transition temperature T_N is evident as a broad shoulder, while the ferromagnetic transition temperature T_C appears as a pronounced peak in $\partial\rho/\partial T$. The kink at T^* is discussed in the text. (b) ρ vs magnetic field H at constant T. The kink at H^* is discussed in the text.

In the vicinity of T_C, $\rho(T)$ is hysteretic ($\Delta T = 0.02$ K) as expected for a first-order transition. At temperatures below T_C, $\rho(T)$ is described by the expression,[35]

$$\rho(T) = \rho_0 + AT^2 + a\Delta T(1 + 2T/\Delta)\exp(-\Delta/T), \quad (5)$$

which accounts for the residual resistivity ρ_0, the Fermi liquid contribution AT^2, and the electron-magnon scattering due to FM magnons where a is a material dependent constant and Δ is the magnon gap. Fits to the data below 7 K using Eq. (5) are shown in Fig. 8(c) and fit results are summarized in Table I. It is noteworthy that from fits to both C_{4f}/T and $\rho(T)$, we find similar values for Δ and, additionally, Δ increases with H as expected for a anisotropic FM system where the magnon gap is given by the expression $\Delta(H) = \Delta + \mu_{\rm eff}H$ (see Ref. 35). At low T, the residual resistivity $\rho_0 = 0.44$ $\mu\Omega$cm, resulting in a residual resistivity ratio RRR $\approx$ 360 for $H = 0$. This large value reflects the high quality of these polycrystalline samples. Finally, we consider the Kadowaki-Woods ratio $R_{\rm KW} = A/\gamma^2$ that gives the relationship between the coefficient γ of the electronic specific heat and the coefficient A of the T^2 contribution to the electrical resistivity. We find that $R_{\rm KW} \approx 1 \times 10^{-5}$ $\mu\Omega$ cm(mol K^2 mJ^{-1})^2, which is close to the expected value for Ce-based compounds with a doublet ground state.[36,37]

In order to track the influence of magnetic field on T_N and T_C, we considered $\partial\rho/\partial T$, where T_N appears as a steplike feature and T_C is evident as a pronounced peak [see Fig. 9(a)]. As seen from measurements of $M(T)/H$ and C/T, T_N remains constant up to 0.4 kOe, above which it broadens significantly and may decrease weakly with increasing H. At the same time, the magnitude of the peak that defines T_C decreases dramatically with increasing H, while the value of T_C weakly decreases, consistent with results from specific heat. However, $\rho(T)$ is hysteretic up to $\approx$1 kOe, suggesting that the FM transition remains first order in this region. From isotherms of the electrical resistivity [see Fig. 9(b)], we additionally were able to observe a feature that only appears for $T_C \leqslant T \leqslant T_N$; i.e., $\rho(H)$ is initially constant with increasing H and then decreases abruptly at a kink denoted as H^*. This field dependence defines a boundary in the T-H phase diagram that coincides with the behavior observed in $M(H)$ that represent a reconfiguration of the spins from AFM to the canted AFM state. This line can also be extracted from $\partial\rho/\partial T$, where we observe an additional kink in the data, denoted as T^*, for $T_C \leqslant T \leqslant T_N$.

IV. DISCUSSION

Our measurements reveal that CeRu$_2$Al$_2$B exhibits complicated magnetic ordering where, for $H = 0$, AFM is observed at $T_N = 14.2$ K and a subsequent first-order FM transition is observed at $T_C = 12.8$ K. We suggest that the magnetic moments are localized and associated with the 4f electrons,

TABLE I. Summary of results from fits to the specific heat divided by temperature C/T and electrical resistivity $\rho(T)$ using Eqs. (4) and (5), as described in the text.

H(kOe)	0	1	5	10	20	30	60	90
γ(mJ/mol K^2)	25.6	...	...	19.2	18.6	18.1	...	...
β(mJ/mol K)	74.8	...	...	70.7	65.2	60.4	...	...
Δ_C(K)	17.6	...	...	18.5	19.3	20.1	...	...
ρ_0($\mu\Omega$cm)	0.44	0.33	0.41	0.61	...	...	3.13	4.50
A($\mu\Omega$cm/K^2)	0.007	0.007	0.0075	0.001	...	...	0.0007	0.0005
a($\mu\Omega$cm/K^2)	0.14	0.14	0.15	0.13	...	...	0.12	0.14
Δ_ρ(K)	17.6	18.0	19.4	17.9	...	...	29.9	43.3

based the following observations: (1) the magnetic entropy reaches $0.88R\ln 2$ at T_N, showing that Kondo interaction is weak by comparison to the RKKY intereaction, (2) C/T saturates toward a value of 25 mJ/mol K^2 at low T, indicating that there is little hybridization between the Ce f-electron states and the conduction electron states, which would result in an enhancement of the quasiparticle effective mass, (3) the saturation moment in the FM state is consistent with a doublet ground state, and (4) $\rho(T)$ does not exhibit typical features associated with Kondo scattering/coherence. However, we additionally point out that although S only reaches $0.88R\ln 2$ at T_N, $\chi(T)$ is described by a Curie-Weiss law that is consistent with occupation of the entire $J = 5/2$ multiplet for $T_N \leqslant T \leqslant 350$ K.

We next find that the application of a small magnetic field results in an unusual phase diagram that includes three magnetically ordered phases including AFM, spin reoriented, and FM where the transition is initially first order and then crosses over to second order with increasing H. The spin reoriented state appears to be FM like. However, since $M(H)$ for $T_C \leqslant T \leqslant T_N$ does not recover the full value of M_s that is observed for $T \leqslant T_C$, we propose that it is a canted antiferromagnet. In addition, the NMR measurement shows that in the paramagnetic state, the spin susceptibility is Ising-like where the easy axis is the c axis.

We suggest two possible scenarios to describe these phenomena. In the first scenario, the spin modulation along the c axis could be caused by the RKKY interaction. In this case, the wave vector of this modulation should be equal to $2k_F$ and, consequently, independent of parameters such as T or H. Here, the spectrum of excitations of the FM phase is gapped. In contrast, the AFM phase has gapless phason modes because the magnetic ordering wave vector is incommensurate. Consequently, the entropic contribution to the free energy should favor the AFM ordering relative to the FM phase. In the second scenario, the spin-density wave along the c axis could be caused by competition between two short-range exchange interactions (e.g., as proposed in the ANNNI model[38]). In this case, the wave vector Q is often sensitive to varying external parameters such as T or H and the main driving factor of this modulation is frustration. On the other hand, the facts that nearly all of $R\ln 2$ is recovered at T_N and $T_N/\Theta \approx 1$ argue against a frustration picture. In order to explore this possibility, we are currently undertaking neutron diffraction measurements to characterize the T and H dependence of the AFM wave vector.

Since $CeRu_2Al_2B$ exhibits local moment behavior, it presumably is far from a QCP in a Doniach-like picture. For this reason, this compound presents the opportunity to tune a well localized AFM/FM state toward a QCP, either through applied pressure or chemical substitution. This approach is particularly attractive if frustration is present. As emphasized by the recent work of Si and Coleman, when quantum frustration is included as an additional axis on the conventional Kondo lattice model, the resulting in a phase diagram includes disorder driven quantum fluctuation and RKKY/Kondo driven QCPs, which separate the AFM from spin and heavy Fermi liquid states, respectively.[19,20] This picture may be applicable to several systems that crystallize on nonfrustrated tetragonal lattices where competing nearest-neighbor interactions produce frustration. For instance, the spin-spiral AFM phase that is observed in $CeRhIn_5$[39] has been described in these terms. Another example is $YbRh_2Si_2$,[40] where the extremely small AFM ordering temperature $T_N \approx 70$ mK has been attributed to quantum frustration. Experiments are currently under way to determine whether frustration plays a role in the complicated magnetic behavior of $CeRu_2Al_2B$.

Finally, we remark that the behavior of $CeRu_2Al_2B$ is similar to that of $CeRu_2Ge_2$, which undergoes a second-order AFM transition at $T_N = 8.55$ K followed by a first-order FM transition at $T_C = 7.40$ K.[16,17] Though $CeRu_2Ge_2$ can be understood as a local moment system, there is a body of work that proposes that a correlated change in magnetic and electronic structures is responsible for the magnetic behavior[18]: i.e., in the AFM phase, the $4f$ electrons are itinerant and produce a heavy-fermion ground state similar to what is observed for $CeRu_2Si_2$. Below T_C, the $4f$ electrons become localized and the Fermi surface resembles that of $CeRu_2Si_2$ following the metamagnetic transition. This picture is attractive, but it has not been definitively established. We suggest that further studies of $CeRu_2Al_2B$ may help to clarify the magnetism and possible correlated electron physics in both compounds.

V. CONCLUSION

Our effort to explore the $LnRu_2Al_2B$ (Ln = La–Sm) family of materials has uncovered a tetragonal Ce-based compound that exhibits complicated local $4f$ moment magnetic ordering at relatively high temperature, where AFM occurs at $T_N = 14.2$ K and a subsequent first-order FM is observed at $T_C = 12.8$ K. An applied magnetic field produces a rich T-H phase diagram that includes a spin-reoriented state that appears to be a canted AFM. In order to clarify the nature of the magnetism, we currently are undertaking neutron scattering experiments that will distinguish between the possible mechanisms for producing this unusual ground state. In addition, it will be rewarding to search for quantum critical behavior, either through chemical substitution or applied pressure, as this compound may provide a model case for studying FM-QCP and/or the influence of quantum disorder starting from an extreme local moment situation.

Note added in proof: Since the submission of this manuscript, we became aware of an independent study by E. Matsuoka addressing, primarily, the zero field properties of $CeRu_2Al_2B$ and $PrRu_2Al_2B$ which will appear in the Journal of the Physical Society of Japan.

ACKNOWLEDGMENTS

We thank J. M. Lawrence, C. D. Batista, and K. Gofryk for stimulating discussions. Work at Los Alamos National Laboratory was performed under the auspices of the US Department of Energy, Office of Basic Energy Sciences, Division of Materials Sciences and Engineering, PECASE funding from the US DOE, OBES, Division of Material Science and Engineering, and funded in part by the Los Alamos Laboratory Directed Research and Development program.

[1] G. R. Stewart, Rev. Mod. Phys. **73**, 797 (2001).
[2] H. v. Löhneysen, A. Rosch, M. Vojta, and P. Wölfle, Rev. Mod. Phys. **79**, 1015 (2007).
[3] C. Pfleiderer, Rev. Mod. Phys. **81**, 1551 (2009).
[4] M. B. Maple, R. E. Baumbach, J. J. Hamlin, D. A. Zocco, B. J. Taylor, N. P. Butch, J. R. Jeffries, S. T. Weir, B. C. Sales, D. Mandrus, M. A. McGuire, A. S. Sefat, R. Jin, Y. K. Vohra, J.-H. Chu, and I. R. Fisher, Physica B **404**, 2924 (2009).
[5] S. Doniach, Physica B + C **91**, 231 (1977).
[6] J. R. Iglesias, C. Lacroix, and B. Coqblin, Phys. Rev. B **56**, 11820 (1997).
[7] J. A. Hertz, Phys. Rev. B **14**, 1165 (1976).
[8] A. J. Millis, Phys. Rev. B **48**, 7183 (1993).
[9] T. Moriya and T. Takimoto, J. Phys. Soc. Jpn. **64**, 960 (1995).
[10] Q. Si, S. Rabello, K. Ingersent, and J. L. Mith, Nature (London) **413**, 804 (2001).
[11] J. V. Zaikina, Y.-J. Jo, and S. E. Latturner, Inorg. Chem. **49**, 2773 (2010).
[12] R. J. Elliott, Phys. Rev. **124**, 346 (1961).
[13] O. Vogt and K. Mattenberger, Physica B **215**, 22 (1995).
[14] D. P. Rojas, J. I. Espeso, J. Rodríguez Fernández, J. C. Gómez Sal, J. Sanchez Marcos, and H. Müller, Phys. Rev. B **80**, 184413 (2009).
[15] D. P. Rojas, J. I. Espeso, J. Rodríguez Fernández, J. C. Gómez Sal, C. Rusu, D. Andreica, R. Dudric, and A. Amato, Phys. Rev. B **84**, 024403 (2011).
[16] H. Wilhelm, K. Alami-Yadri, B. Revaz, and D. Jaccard, Phys. Rev. B **59**, 3651 (1999).
[17] S. Süllow, M. C. Aronson, B. D. Rainford, and P. Haen, Phys. Rev. Lett. **82**, 2963 (1999).
[18] S. Raymond, P. Haen, R. Calemczuk, S. Kambe, B. Fak, P. Lejay, T. Fukuhara, and J. Flouquet, J. Phys. Condens. Matter **11**, 5547 (1999).
[19] Q. Si, Physica B **378**, 23 (2006).
[20] P. Coleman and A. H. Nevidomskyy, J. Low Temp. Phys. **161**, 182 (2010); and references therein.
[21] J. Larrea, M. B. Fontes, A. D. Alvarenga, E. M. Baggio-Saitovitch, T. Burghardt, A. Eichler, and M. A. Continentino, Phys. Rev. B **72**, 035129 (2005).
[22] S. Drotziger, C. Pfleiderer, M. Uhlarz, H. v. Löhneysen, D. Souptel, W. Löser, and G. Behr, Phys. Rev. B **73**, 214413 (2006).
[23] V. A. Sidorov, E. D. Bauer, N. A. Frederick, J. R. Jeffries, S. Nakatsuji, N. O. Moreno, J. D. Thompson, M. B. Maple, and Z. Fisk, Phys. Rev. B **67**, 224419 (2003).
[24] C. Krellner, N. S. Kini, E. M. Brüning, K. Koch, H. Rosner, M. Nicklas, M. Baenitz, and C. Geibel, Phys. Rev. B **76**, 104418 (2007).
[25] S. S. Saxena, P. Agarwal, K. Ahilan, F. M. Grosche, R. K. W. Haselwimmer, M. J. Steiner, E. Pugh, I. R. Walker, S. R. Julian, P. Monthoux, G. G. Lonzarich, A. Huxley, I. Sheikin, D. Braithwaite, and J. Flouquet, Nature (London) **406**, 587 (2000).
[26] D. Aoki, A. Huxley, E. Ressouche, D. Braithwaite, J. Flouquet, J.-P. Brison, E. Lhotel, and C. Paulsen, Nature (London) **413**, 613 (2001).
[27] T. Akazawa, H. Hidaka, H. Kotegawa, T. C. Kobayashi, T. Fujiwara, E. Yamamoto, Y. Haga, R. Settai, and Y. Onuki, J. Phys. Soc. Jpn. **73**, 3129 (2004).
[28] P. Gegenwart, J. Custers, Y. Tokiwa, C. Geibel, and F. Steglich, Phys. Rev. Lett. **94**, 076402 (2005).
[29] O. Stockert, M. M. Koza, J. Ferstl, C. Geibel, and F. Steglich, Sci. Technol.: Adv. Mater. **8**, 371 (2007).
[30] S. J. Yamamoto and Q. Si, Proc. Natl. Acad. Sci. USA **107**, 15704 (2010).
[31] H. M. Rietveld, J. Appl. Chryst. **2**, 65 (1969).
[32] A. Larson and R. V. Dreele, Los Alamos National Laboratory Report LAUR 86-748 , 2000 (unpublished).
[33] A. Abragam, *The Principles of Nuclear Magnetism* (Oxford University Press, London, 1961).
[34] B. Coqblin, *The Electronic Structures of Rare Earth Metals and Alloys: the Magnetic Heavy Rare Earths*, edited by B. Coqblin (Academic, New York, 1977).
[35] M. B. Fontes, J. C. Trochez, B. Giordanengo, S. L. Bud'ko, D. R. Sanchez, E. M. Baggio-Saitovitch, and M. A. Continentino, Phys. Rev. B **60**, 6781 (1999).
[36] K. Kadowaki and S. B. Woods, Solid State Commun. **58**, 507 (1986).
[37] N. Tsujii, H. Kontani, and K. Yoshimura, Phys. Rev. Lett. **94**, 057201 (2005).
[38] W. Selke and P. M. Duxbury, Z. Phys. B **57**, 49 (1984).
[39] T. Park, V. A. Sidorov, F. Ronning, J.-X. Zhu, Y. Tokiwa, H. Lee, E. D. Bauer, R. Movshovich, J. L. Sarrao, and J. D. Thompson, Nature (London) **465**, 366 (2008).
[40] O. Trovarelli, C. Geibel, S. Mederle, C. Langhammer, F. M. Grosche, P. Gegenwart, M. Lang, G. Sparn, and F. Steglich, Phys. Rev. Lett. **85**, 626 (2000).